European Journal of Mechanics B/Fluids 61 (2017) 125–134

Contents lists available at ScienceDirect

European Journal of Mechanics B/Fluids

journal homepage: www.elsevier.com/locate/ejmflu

Unsteady turbulence, dynamic similarity and scale effects in bores and positive surges

Xinqian Leng, Hubert Chanson *

The University of Queensland, School of Civil Engineering, Brisbane QLD 4072, Australia

HIGHLIGHTS

- Instantaneous free-surface and velocity properties were measured in propagating bores.
- Intense turbulent mixing was observed under breaking and undular tidal bores.
- Unsteady dimensionless properties were compared based upon a Froude and Morton similitude.
- Several parameters were affected by scale effects, including velocity and Reynolds stress fluctuations.
- Results point to the need for detailed field measurements.

ARTICLE INFO

Article history:
Received 8 September 2015
Received in revised form
20 March 2016
Accepted 16 September 2016
Available online 22 September 2016

Keywords:
Unsteady turbulence
Dynamic similarity
Scale effects
Bores and surges
Free-surface flow properties
Froude similitude

ABSTRACT

A tidal bore is a positive surge or compression wave formed in an estuarine system during the early flood tide under macro-tidal conditions. A series of physical experiments were conducted in a large facility to investigate the unsteady free-surface properties, velocity characteristics and Reynolds shear stresses. Both instantaneous and ensemble-averaged measurements were performed. The results demonstrated the intense turbulence and turbulent mixing under breaking and undular tidal bores. A range of dimensionless unsteady turbulent properties were carefully compared based upon both Froude and Morton similitudes with two different Reynolds number ranges. The data showed that several parameters were affected by scale effects, including velocity and Reynolds stress fluctuations during the bore propagation. The finding implies that laboratory study data might not be up-scaled to prototype conditions without some form of scale effects.

1. Introduction

A positive surge or bore is an unsteady open channel flow motion characterised by a sudden increase in water depth [1]. It is also called a hydraulic jump in translation [2–4]. The bore front constitutes a hydrodynamic shock with a discontinuity in terms of water depth and pressure and velocity fields [5]. A typical geophysical application is a tidal bore propagating upstream in an estuarine zone [6,7] (Fig. 1). Fig. 1 presents two occurrences of tidal bores. A tidal bore is essentially a compression wave formed in an estuary under large tidal range in a narrow funnelled mouth during the early flood tide, under relatively low freshwater flows. For a hydraulic jump in translation, the equations of conservation of mass and momentum in their integral form give a relationship between the Froude number and the ratio of conjugate cross-section areas:

$$Fr_1 = \frac{(V_1 + U)}{\sqrt{g \times \frac{A_1}{B_1}}} = \sqrt{\frac{1}{2} \times \frac{A_2}{A_1} \times \frac{B_1}{B^\#} \times \left(\left(2 - \frac{B'}{B^\#}\right) + \frac{B'}{B^\#} \times \frac{A_2}{A_1}\right) + \frac{A_2}{A_2 - A_1} \times \frac{F_{fric} - W \times S_o}{\rho \times g \times \frac{A_1^2}{B^\#}}} \quad (1)$$

where V is the flow velocity, A is the cross-section area, B is the free-surface width, the subscripts 1 and 2 refer to the initial flow conditions and conjugate flow conditions respectively (Fig. 2), U is the celerity positive upstream, ρ is the fluid density, g is the gravity acceleration, F_{fric} is the friction force, W is the control volume weight and S_o is the bed slope, while $B^\#$ and B' are characteristic

* Corresponding author. Fax: +61 7 33 65 45 99.
E-mail address: h.chanson@uq.edu.au (H. Chanson).

http://dx.doi.org/10.1016/j.euromechflu.2016.09.017
0997-7546/

(A) Undular tidal bore of the Dordogne River at Port de St Pardon (France) on 24 August 2013—Most surfers and kayakers are surfing ahead of the first wave crest.

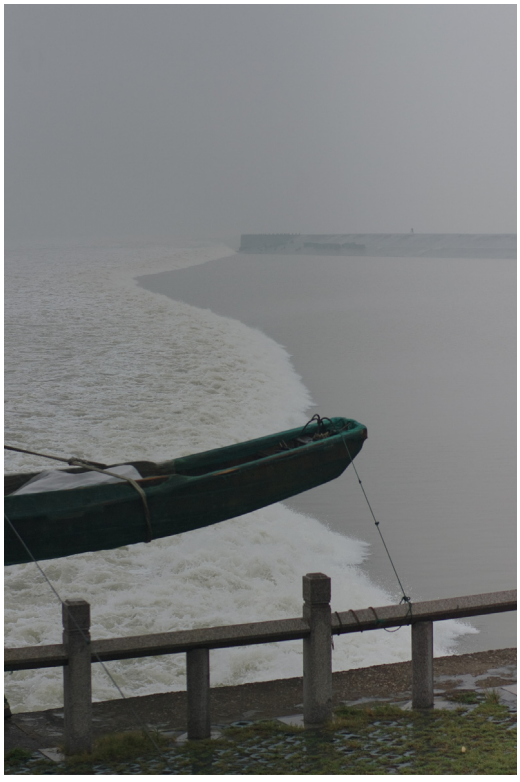

(B) Breaking tidal bore in the Qiantang River at Laoyanchang (China) on 6 September 2013.

Fig. 1. Tidal bores in natural environments—Bore propagation from left to right.

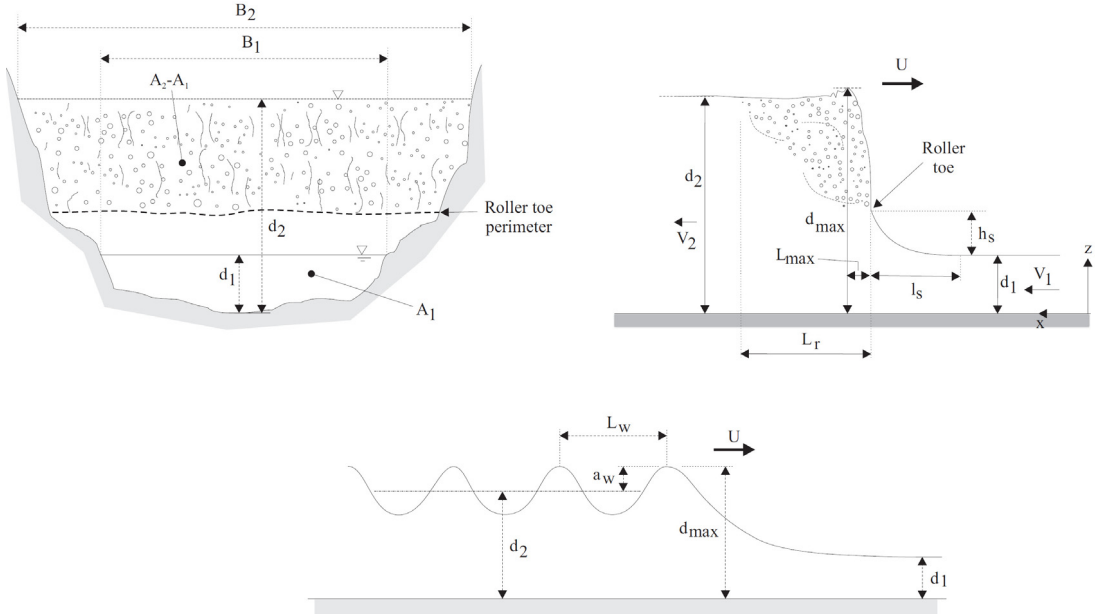

Fig. 2. Definition sketch of breaking and undular bores.

channel widths functions of the cross-sectional shape:

$$B^{\#} = \frac{A_2 - A_1}{d_2 - d_1} \tag{2}$$

$$B' = \frac{\int_{A_1}^{A_2} \int \rho \times g \times (d_2 - z) \times dA}{\frac{1}{2} \times \rho \times g \times (d_2 - d_1)^2} \tag{3}$$

with d the flow depth and z the vertical elevation (Fig. 2). Eq. (1) is a general expression for the bore propagation in an irregular cross-sectional channel [8,9]. For a smooth rectangular horizontal channel, it yields the Bélanger equation:

$$Fr_1 = \sqrt{\frac{1}{2} \times \frac{d_2}{d_1} \times \left(1 + \frac{d_2}{d_1}\right)} \tag{4}$$

where d_1 is the inflow depth and d_2 is the conjugate flow depth [10,6].

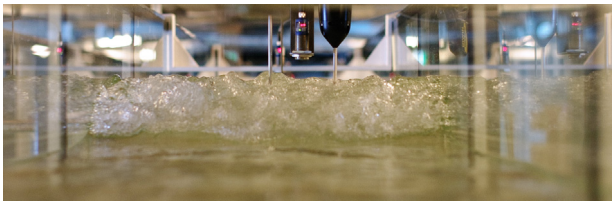

Fig. 3. Looking downstream at incoming bore roller—Flow conditions: $d_1 = 0.175$ m, $Q = 0.101$ m^3/s, $\theta = 0$, $Fr_1 = 1.5$, $Re = 3.5 \times 10^5$, breaking bore propagation from background to foreground.

The shape of the positive surge is closely associated to its Froude number Fr_1. For $1 < Fr_1 < 1.2$ to 1.3, an undular bore is observed, associated with a smooth first wave crest and a train of secondary quasi-periodic undulations [11–13] (Fig. 1(A)). For $1.3 < Fr_1 < 1.4$, some slight breaking takes place at the first crest, although it does not extend to the whole channel width. For $Fr_1 > 1.4$ to 1.5, a breaking bore occurs (Fig. 1(B)). The bore propagation was associated with an abrupt increase in free-surface elevation during the passage of the breaking roller [6,14,9].

In the present study, the instantaneous free-surface and velocity properties of undular and breaking tidal bores were studied experimentally (Fig. 3). Detailed turbulence data were collected in a relatively large-size rectangular channel. The measurements were conducted for several discharges; each experiment was repeated 25 times and the data were ensemble-averaged. The results included instantaneous velocity and turbulent stress fluctuations. Some detailed comparison was performed between experimental results obtained with identical Froude numbers but different Reynolds numbers. The results were used to test the validity of the Froude similarity, and possible scale effects. The comparative analysis provides an assessment of scale effects affecting the instantaneous velocity properties during bore propagation.

2. Dimensional analysis and similitude

Considering a tidal bore propagating upstream in an irregular channel (Fig. 2), a dimensional analysis gives a series of dimensionless relationships between the instantaneous turbulent properties at a location (x, y, z) at a time t and the boundary conditions, inflow properties and fluid properties. It yields:

$$\frac{d}{d_1}, \frac{\vec{V}}{V_1}, \frac{P}{\rho \times g \times d_1}, \frac{\|\tau\|}{\rho \times V_1^2} = F_1\left(\frac{x}{\frac{A_1}{B_1}}, \frac{y}{\frac{A_1}{B_1}}, \frac{z}{\frac{A_1}{B_1}}, t \times \sqrt{\frac{g}{\frac{A_1}{B_1}}}, \frac{V_1+U}{\sqrt{g \times \frac{A_1}{B_1}}}, \rho \times \frac{(V_1+U) \times \frac{A_1}{B_1}}{\mu}, \frac{d_1}{\frac{A_1}{B_1}}, S_o, \frac{k_s}{\frac{A_1}{B_1}}, \frac{g \times \mu^4}{\rho \times \sigma^3}, \ldots\right) \quad (5)$$

where d is the instantaneous water depth, $\vec{V}$ is the instantaneous velocity vector of components V_x, V_y, V_z, respectively the longitudinal, transverse and vertical velocity components, P is the instantaneous pressure, $\|\tau\|$ is the instantaneous Reynolds stress tensor, x is the coordinate in the flow direction, y is the horizontal transverse coordinate measured from the channel centreline, z is the vertical coordinate measured from channel bed, t is the time, $S_o = \sin\theta$ with θ the angle between bed slope ad horizontal, k_s is the equivalent sand roughness height of the channel bed, μ is the water dynamic viscosity and σ is the surface tension between air and water. In Eq. (5), the instantaneous turbulent flow properties at a point and time are expressed as functions of the tidal bore properties, initial flow properties (subscript 1), channel geometry and fluid properties. The fifth and sixth terms are the tidal bore Froude Fr_1 and Reynolds Re numbers respectively, and the tenth term is the Morton number Mo which is a function of fluid properties and gravity constant only. In addition, the biochemical properties of the water solution may be considered especially in natural estuarine systems, as well as sediment characteristics and bubble characteristics for a breaking bore. Note that brackish nature of the water and the variation with time of its properties might be relevant in estuarine bores.

In the present study, the same fluids (air and water) were used in model and prototype, and this added a dimensional constraint: i.e., the Morton number became an invariant. Similarly, the rectangular channel width B and bed roughness k_s were kept constant during the experiments and the measurements were conducted on the channel centreline. Hence Eq. (5) may be simplified for a tidal bore in a rectangular prismatic channel into:

$$\frac{d}{d_1}, \frac{V_i}{V_1}, \frac{P}{\rho \times g \times d_1}, \frac{\tau_{ij}}{\rho \times V_1^2} = F_2\left(\frac{x}{d_1}, \frac{z}{d_1}, t \times \sqrt{\frac{g}{d_1}}, \frac{V_1+U}{\sqrt{g \times d_1}}, \rho \times \frac{(V_1+U) \times d_1}{\mu}, \frac{B}{d_1}, S_o, \frac{k_s}{d_1}, \frac{g \times \mu^4}{\rho \times \sigma^3}, \frac{V_1+U}{\sqrt{g \times d_1}}, \ldots\right) \quad (6)$$

where $i, j = x, y, z$.

In hydraulic jumps and tidal bores, a Froude similitude is derived theoretically [2,5,8,9]. That is, the model and prototype Froude numbers must be equal. Fig. 1 illustrates the intense turbulent mixing induced by a bore in a natural system. The turbulent processes are affected by viscous forces implying the needs for a Reynolds similitude. In a geometrically similar model, a true dynamic similarity is achieved only if each dimensionless term has the same value in both model and prototype. Scale effects may exist when one or more dimensionless terms have different values between field and laboratory. For geometrically-similar models, it is impossible to satisfy simultaneously all the similarities because of too many relevant parameters Eq. (6).

In the present study, both Froude and Morton similitudes were adopted following Hornung et al. [14] and Docherty and Chanson [15], namely because of theoretical and economical considerations. Yet few systematic studies were conducted to date to assess the scale effects affecting the turbulent mixing in tidal bore flows. Herein the effects of the Reynolds number on the instantaneous turbulent flow properties were tested systematically.

It is worth noting that the above analysis (Eq. (6)) does not account for the physio-chemical properties of the water, the sedimentary processes, the air entrainment in the bore roller and the characteristics of the instrumentation. All of these affect the development and the characteristics of a tidal bore, including water column stratification, sediment scour and suspension. The size of the probe sensor, the sampling rate and possibly other probe characteristics do affect the minimum turbulent length and time scales detectable by the instrumentation. For example, in the particular case of intrusive ADV probe, the sampling volume may be larger than the smallest vortical structures.

3. Experimental apparatus and procedure

3.1. Experimental channel and instrumentation

New experiments were conducted in a large tilting channel, made of glass sidewalls and smooth PVC bed. The facility was first used by and full details are reported in [9,16]. The initially steady

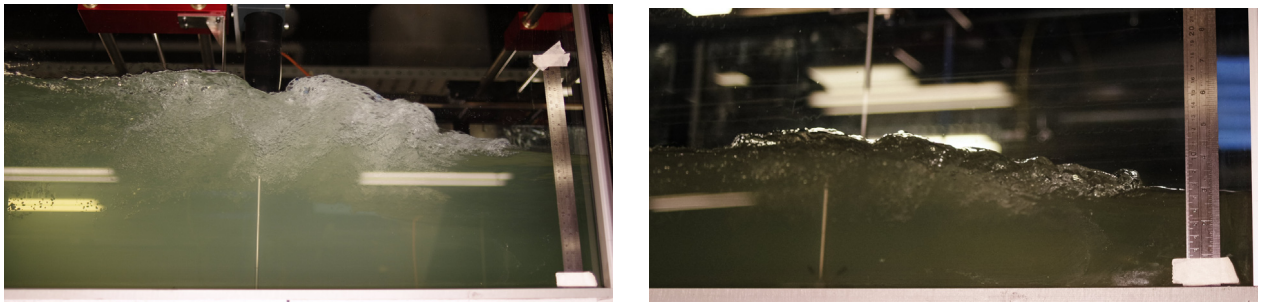

(A) $d_1 = 0.175$ m, $Q = 0.101$ m^3/s, $\theta = 0$, $Fr_1 = 1.5$, $Re = 3.5 \times 10^5$. (B) $d_1 = 0.075$ m, $Q = 0.055$ m^3/s, $\theta = 0$, $Fr_1 = 1.5$, $Re = 9.6 \times 10^4$.

Fig. 4. Breaking bore propagation (from left to right)—Note the metallic ruler on the far right for scaling.

flow was delivered into an upstream intake channel and led to the 19 long 0.7 m wide glass sidewalled test section through a series of flow straighteners followed by a smooth bed and sidewall convergent. A fast-closing Tainter gate was located next to the test section's downstream end ($x = 18.1$ m), where x is the horizontal distance from the upstream end of the test section. A radial gate was located further downstream ($x = 18.88$ m), followed by a free overfall.

In steady flows, the water depths were measured using pointer gauges. The unsteady water depths were recorded non-intrusively using a series of acoustic displacement meters. A Microsonic™ Mic+35/IU/TC sensor was located at $x = 18.17$ m immediately downstream of the Tainter gate. Nine acoustic displacement meters Microsonic™ Mic+25/IU/TC were spaced along the channel between $x = 0.96$ and 17.81 m. All acoustic displacement meters (ADMs) were calibrated against the pointer gauge in steady flows. The velocity measurements were conducted with an acoustic Doppler velocimeter (ADV) Nortek™Vectrino+ (Serial No. VNO 0436) equipped with a three-dimensional sidelooking head. The ADV was located at $x = 8.5$ m on the channel centreline. The velocity range was ± 1.0 m/s and the data accuracy was 1% of the velocity range. The ADV was set up with a transmit length of 0.3 mm and a sampling volume of 1.5 mm height. Both the acoustic displacement meters and acoustic Doppler velocimeter were synchronised within ± 1 ms and sampled simultaneously at 200 Hz. In steady flows, the ADV post processing included the removal of communication errors, the removal of average signal to noise ratio data less than 5 dB and the removal of average correlation values less than 60%. In addition, the phase-space thresholding technique developed by Goring and Nikora [17] and implemented by Wahl [18] was used to remove spurious points in the data set. In unsteady flow conditions, the above post-processing technique was not applicable [19,20]. The unsteady flow post-processing was limited to a removal of communication errors, and it is acknowledged that the vertical velocity component V_z data might be affected adversely by the bed proximity for $z < 0.030$ m.

Additional photographic informations were recorded with a dSLR camera Pentax K-3 (6016 × 4000 pixels) and a digital camera Casio Exilim EX-10, in movie mode set at 120 fps (640 × 480 pixels) or 240 fps (512 × 384 pixels).

3.2. Experimental procedure

For all experiments, the positive surges were generated by the fast closure of the Tainter gate and the compression wave propagated upstream against the initially-steady flow. Figs. 3 and 4 illustrate some photographs of advancing bores. For the breaking bore experiments, the radial gate was fully opened; the bore was generated by the rapid closure of the Tainter gate. The gate closure time was less than 0.15 and 0.2 s and was small enough to have a negligible effect on the surge propagation. For the generation of undular bores, the radial gate was initially partially closed to raise the initial water depth d_1. The bores were generated by the rapid closure of the Tainter gate. For all experiments, the instruments were started 60 s before gate closure, the discharge was kept constant during an experiment, and sampling stopped when the bore reached the upstream intake.

Since the bore propagation is a highly unsteady turbulent process, any time average would be meaningless to study the turbulent free-surface and velocity characteristics. A series of ensemble-average measurements were conducted for two different discharges (Table 1). When the experiment is repeated N times, the ensemble-average of a variable V at time t and location (x, y, x) is:

$$V(t, x, y, z) = \frac{1}{N} \times \sum_{i=1}^{N} V_i(t, x, y, z) \quad (7)$$

where V_i is the observation during the run i and $N = 25$ herein.

Both breaking and undular bores were generated for each discharge. A total of 25 runs were repeated for each ensemble-average experiment. For each set of experiments, the results were ensemble-averaged to obtain the instantaneous median property (e.g. free-surface elevation d_{median}) and the instantaneous difference between the third and first quartiles: e.g., $(d_{75} - d_{25})$ for the water depth fluctuations. The difference between the third and first quartiles characterised the instantaneous fluctuations and would be equal to 1.3 times the standard deviation of the total ensemble for a Gaussian distribution [23]. The data were processed following [15], and results are presented below in terms of instantaneous median and fluctuating properties.

4. Basic flow patterns and experimental results

Visual, video and photographic observations were conducted for a range of Froude numbers. Figs. 3 and 4 show photographs of breaking bore propagations. No bore was visible for a Froude number less than unity. Undular bores were observed for $1 < Fr_1 < 1.1$ to 1.3: the front of the bore was smooth with a gentle upward free-surface rise followed a series of quasi two-dimensional smooth secondary undulations. Breaking bores with secondary waves were seen for 1.2 to 1.3 $< Fr_1 <$ 1.4 to 1.5. The bore front had a thin breaker developing across most of the channel width, followed by a train of three-dimensional secondary waves. The expression "*breaking bore with secondary waves*" is used herein in line with [12]; other researchers called this an "*undular bore with some breaking*" [19,24]. A breaking bore was observed for $Fr_1 > 1.4$ to 1.5, with a quasi-two-dimensional marked roller. The advancing roller was preceded by an upward free-surface curvature immediately before the roller toe. The bore front was a steep wall of water with a sharp breaking front (Fig. 3). The roller toe was a flow singularity where vorticity was generated and air was entrapped [14,25].

Table 1
Systematic laboratory investigations of tidal bores at different geometric scales.

Reference	S_o	Bed type	Q (m^3/s)	d_1 (m)	V_1 (m/s)	Fr_1	Re	$\frac{B}{d_1}$	$\frac{k_s}{d_1}$	Velocimeter & sampling rate Hz	Tested parameters
Present study	0	PVC	0.055	0.200	0.39	1.19	3.3×10^5	3.50	0	ADV, 200	Free-surface, Velocity,
	0	PVC	0.101	0.210	0.69	1.18	3.5×10^5	3.33	0		Shear stress, Shear stress
	0.0005	PVC	0.055	0.075	1.12	1.5	9.6×10^4	10.0	0		Fluctuations (EA)
	0	PVC	0.101	0.175	0.80	1.5	3.5×10^5	3.89	0		
Simon & Chanson [21]	0.0077	Gravel	0.036	0.084	0.86	1.33	1.0×10^5	5.95	0.040	ADV, 200	Free-surface, Velocity,
			0.055	0.110	1.00	1.35	1.5×10^5	4.55	0.031		Shear stress (EA)
	0.0077	Gravel	0.036	0.084	0.86	1.64	1.2×10^5	5.95	0.040		
			0.055	0.110	1.00	1.64	1.9×10^5	4.55	0.031		
Other studies											
Koch & Chanson [19]	0	PVC	0.040	0.079	1.01	1.42	9.8×10^4	6.33	0	ADV, 50	Free-surface, Velocity (VITA)
Chanson & Docherty [15]	0	PVC	0.050	0.118	0.85	1.59	2.0×10^5	4.24	0	ADV, 200	Free-surface, Velocity, Shear stress (VITA & EA)
Chanson [20]	0	PVC	0.058	0.139	0.84	1.49	2.4×10^5	3.60	0	ADV, 200	Free-surface, Velocity (VITA)
Chanson & Toi [22]	0.0035	PVC	0.025	0.051	0.98	1.77	6.3×10^4	9.84	0	ADV, 200	Free-surface, Velocity (VITA)
Koch & Chanson [19]	0	PVC	0.040	0.079	1.01	1.77	1.2×10^5	6.33	0	ADV, 50	Free-surface, Velocity (VITA)

Notes: EA: ensemble-averaging; VITA: variable interval time averaging.

The instantaneous toe perimeter constantly changed in shape, exhibiting a broad range of instantaneous patterns [9]. While the breaking roller and roller toe were quasi two-dimensional on average, the three-dimensional shape of the roller fluctuated rapidly with time and showed the existence of three-dimensional bubbly structures, as illustrated in [26].

The ensemble-averaged free-surface data highlighted the abrupt increase in water level associated with the passage of a breaking bore roller, and a significant upward free-surface curvature with an undular bore, followed by a train of secondary undulations. Fig. 5 presents some typical ensemble-averaged data in terms of the free-surface elevation and fluctuations at several longitudinal locations. In Fig. 5 and others, the time $t = 0$ corresponds to the Tainter gate closure, and the solid black line denotes the ensemble-averaged median free-surface elevation at $x = 8.5$ m. The free-surface fluctuations were quantified in terms of the difference between the third and first quartiles $d_{75} - d_{25}$. For all the experimental conditions, the results showed a sharp increase in free-surface fluctuations with the passage of a tidal bore. With breaking tidal bores, the free-surface fluctuations showed a marked maximum $(d_{75} - d_{25})_{max}$ shortly after the passage of the bore breaking roller (Fig. 5). With undular tidal bores, the first local maximum in free-surface fluctuations occurred shortly after the passage of the first wave crest, followed by a series of local maximum fluctuations appearing in a quasi-periodic manner during the secondary wave motion. The time-variations of free-surface fluctuations in undular bores oscillated approximately in phase with the oscillations of the free-surface elevation. Generally the propagation of a breaking bore was associated with higher maximum free-surface fluctuations than for an undular bore. For all experiments, a time lag Δt was observed between the arrival of the breaking bore roller and the occurrence of the maximum free-surface fluctuation at all longitudinal locations, as seen in Fig. 5.

A number of ensemble-averaged velocity measurements were conducted at $x = 8.5$ m with both breaking and undular bores. The

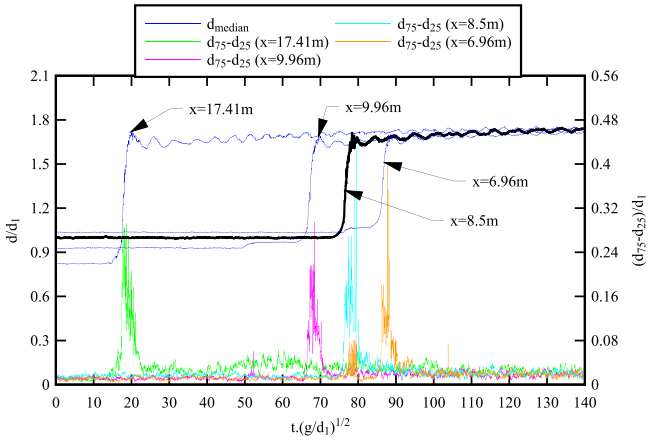

Fig. 5. Ensemble-averaged time variations of the median free-surface elevations and free-surface fluctuations at different longitudinal locations for a breaking bore ($Q = 0.101$ m^3/s, $Fr_1 = 1.5$, $Re = 3.5 \times 10^5$). Thin blue lines show the water depth at three different locations ($x = 17.41$ m, 9.96 m and 6.96 m), and black line shows the water depth at $x = 8.5$ m (ADV location). (For interpretation of the references to colour in this figure legend, the reader is referred to the web version of this article.)

measurements were performed at three vertical elevations $z/d_1 = 0.1$, 0.4, and 0.8, where d_1 is the initial steady flow water depth. For each controlled flow condition, experiments were repeated 25 times and the results were ensemble-averaged. Fig. 6 presents some typical ensemble-averaged velocity data for both breaking and undular bores, with the ensemble-averaged median water depth at the velocity sampling location as reference, highlighted by the black solid line. The turbulent velocity fluctuations were characterised by the difference between the third and first quartile $V_{75} - V_{25}$ of the total ensemble. For both breaking and undular bores, the data showed a rapid deceleration of the longitudinal velocity component V_x at all vertical elevations (Fig. 6). Next to the bed, a transient recirculation was observed in breaking

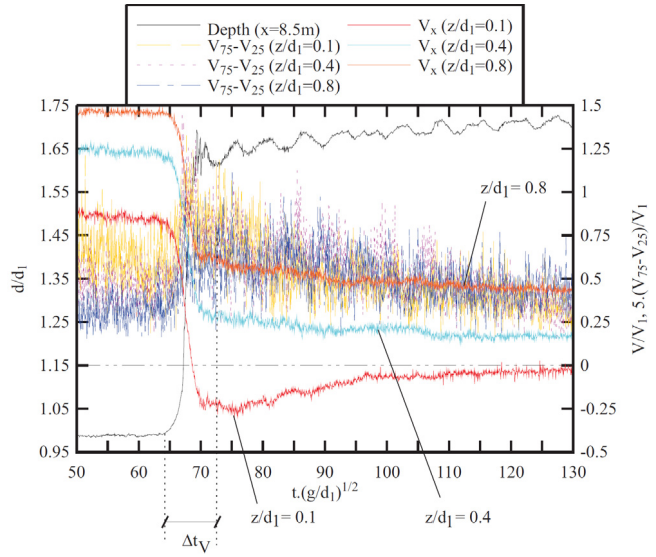

(A) Breaking bore: $Q = 0.101$ m^3/s, $Fr_1 = 1.5$, $Re = 3.5 \times 10^5$.

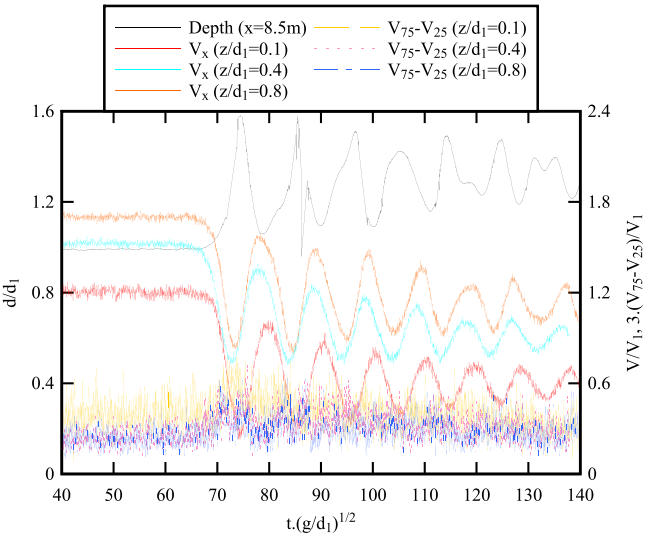

(B) Undular bore: $Q = 0.101$ m^3/s, $Fr_1 = 1.2$, $Re = 3.5 \times 10^5$.

Fig. 6. Time-variations of ensemble-averaged longitudinal velocity components and velocity fluctuations ($V_{75} - V_{25}$) at different vertical elevations z/d_1 in tidal bores—Velocity data offset by +0.2 for all elevations.

bores (Fig. 6(A), $67 < t \times (g/d_1)^{1/2} < 100$), consistent with earlier field and laboratory data [19,22]. The data indicated an abrupt acceleration and then deceleration of the vertical velocity component V_z, this effect being more important at higher vertical elevations. For all flow conditions, the results showed an increase in velocity fluctuations for all three velocity components at all elevations associated with the passage of both types of bores. At lower vertical elevations ($z/d_1 = 0.1$), higher velocity fluctuations were observed and the vertical velocity fluctuations were overall higher than the other two components for the same flow condition, most remarkably seen in the upper water column ($z/d_1 = 0.8$). In breaking bores, marked peaks in fluctuations of all three velocity components occurred slightly after the arrival of the bore front, whereas in undular bores, local maximum fluctuations appeared repetitively following the train of undulations. The results highlighted that the vertical velocity component was typically associated with the largest magnitude in maximum fluctuations. For the same velocity component, breaking bores with higher Froude numbers tended to have higher values of maximum fluctuations than undular bores or breaking bore of lower Froude numbers. The time lag Δt_V, defined as the time difference between the arrival of the breaking bore roller and the occurrence of the maximum velocity fluctuation, was slightly larger in the upper water column comparing to that observed in mid and lower water columns.

The turbulent Reynolds stress tensor was calculated based upon the deviation between the measured instantaneous velocity and the ensemble-average median:

$$v = V - V_{median} \quad (8)$$

where v is the instantaneous velocity fluctuation, V is the (measured) instantaneous velocity and V_{median} is the ensemble-average median velocity. Fig. 7 presents typical time variations of the ensemble-averaged Reynolds stresses, the third quartile of the normal stresses (e.g. $(v_x v_x)_{75}$) and the difference between the third and first quartiles of the tangential stresses (e.g. $(v_x v_y)_{75} - (v_x v_y)_{25}$) for a breaking bore and undular bore, respectively. The solid black line denotes the ensemble-median free-surface elevation. The third quartile of the normal stresses and the difference between the third and first quartiles of the tangential stresses characterised the instantaneous fluctuations in shear stresses during the propagation of a tidal bore. Overall, the results suggested that the propagation of a breaking bore was associated with significant increase in magnitudes and fluctuations of both normal and tangential Reynolds stresses for all vertical elevations over the range of Froude numbers. Maximum stresses in terms of both normal and tangential stress components were observed shortly after the passage of the bore breaking roller. The Reynolds stress data for an undular bore showed a similar trend to that of breaking bores, but with less pronounced peaks in the normal stress tensors. The stress magnitudes were smaller in undular bores comparing to breaking bores with the same discharge. Maximum instantaneous shear stresses were observed to occur shortly after the rise of the free-surface with instantaneous magnitudes of up to 90 Pa within the range of experimental flow conditions. The data indicated the potential of sediment motion to occur beneath a tidal bore, as documented in the field [27–29]. For example, large particles of up to 50 mm in size could be transported into motion under a maximum instantaneous shear stress of 90 Pa for non-cohesive particles [30,31].

5. Dynamic similarity in unsteady turbulent flow properties

5.1. Presentation

In a natural environment, the tidal bore motion corresponds to Reynolds numbers within 10^5 for the smaller systems to in excess of 10^7 for the larger rivers. For example, in Fig. 1, the Reynolds number of the tidal bores was about 5×10^6 to 10^7. In laboratory, the flow conditions correspond usually to Reynolds numbers between 10^3 and 10^5, and systematic unsteady turbulent measurements in tidal bores are rare (Table 1). Table 1 summarises the experimental flow conditions of systematic investigations of tidal bore flow properties, at the millimetric scale, in geometrically similar models under controlled flow conditions to assess the associated scale effects. All studies were conducted based upon a Froude similitude, but with different initial and boundary conditions. None of the arrangements reproduced the tidal bore motion in a natural estuary, where the initial ebb flow velocity V_1 is positive downstream and the flood flow velocity V_2 behind the bore is typically positive upstream.

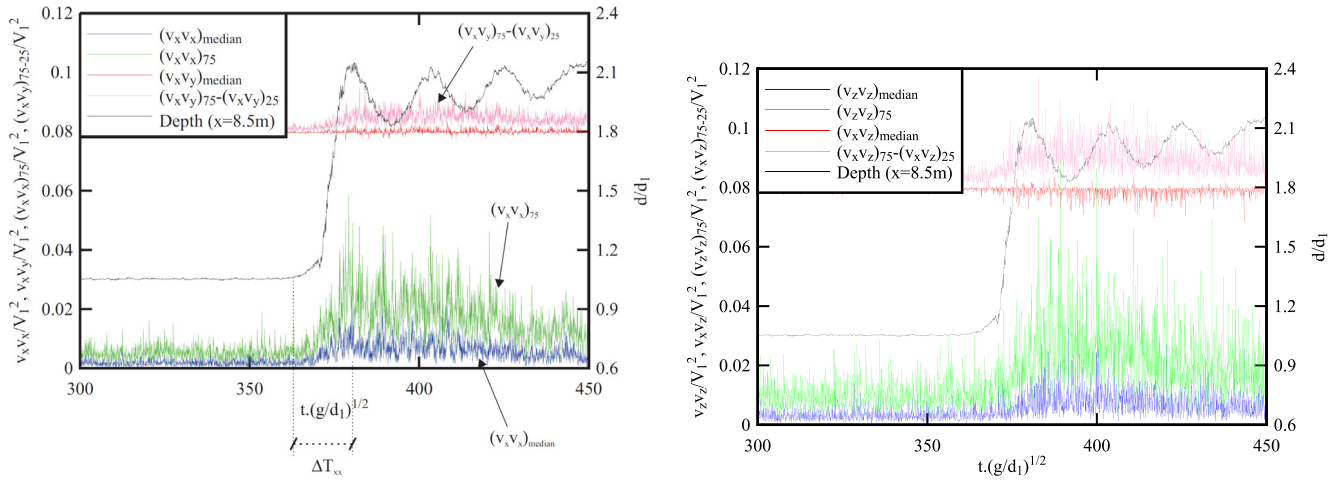

(A) $v_x v_x$ and $v_x v_y$. (B) $v_z v_z$ and $v_x v_z$.

Fig. 7. Time-variations of ensemble-averaged median Reynolds stresses, normal and tangential stress fluctuations and median free-surface elevation in a breaking bore: $Q = 0.055$ m^3/s, $Fr_1 = 1.5$, $Re = 9.6 \times 10^4$, $z/d_1 = 0.4$, $x = 8.5$ m—Tangential stresses offset by +0.08.

Table 2
Summary of scale effects affecting the physical modelling of tidal bores based upon Froude and Morton number similitude (Present study).

Unsteady turbulent properties	Criterion to minimise scale effects	Remarks
Conjugate water depth (d_2)	N/A	No major scale effects for $Re > 9.6 \times 10^4$
Wave amplitude of undular bores (a_w)	N/A	No major scale effects for $Re > 9.6 \times 10^4$
Wave length of undular bores (L_w)	N/A	No major scale effects for $Re > 9.6 \times 10^4$
Maximum water depth (d_{max})	N/A	No major scale effects for $Re > 9.6 \times 10^4$
Height of free-surface rise upstream of the breaking roller toe (h_s)	$L_{scale} = 1$	Scale effects unless at full-scale.
Length of free-surface rise upstream of the breaking roller toe (l_s)	$Re > 9.6 \times 10^4$	Little difference within the experimental conditions.
Length of the breaking bore roller (L_r)	$L_{scale} = 1$	Scale effects unless at full-scale.
Maximum free-surface fluctuation ($d_{75} - d_{25}$) and time lag (Δt)	$L_{scale} = 1$	Scale effects unless at full-scale.
Maximum velocity fluctuation ($V_{75} - V_{25}$) and time lag (Δt_v)	$L_{scale} = 1$	Scale effects unless at full-scale for all velocity components.
Maximum longitudinal velocity deceleration $(\partial V_x/\partial t)_{max}$	$z/d_1 > 0.4$: $Re > 9.6 \times 10^4$	Minimum scale effects for $z/d_1 > 0.4$.
	$z/d_1 < 0.4$: $L_{scale} = 1$	Scale effects unless at full-scale.
Maximum Reynolds stress $(v_i v_j)_{max}$ and time lag ΔT_{ij}	$L_{scale} = 1$	Scale effects unless at full-scale for all Reynolds stress tensor components.
Recirculation velocity (V_{recirc})	$L_{scale} = 1$	Scale effects unless at full-scale.

Notes: L_{scale}: geometric scaling ratio; results obtained with undular and breaking bores.

5.2. Froude similitude

Herein the free-surface properties, instantaneous velocity and velocity fluctuations, instantaneous shear stresses and shear stress fluctuations were tested systematically for two Froude numbers ($Fr_1 = 1.5$ and 1.2) with two different initial discharges: $Q = 0.055$ and 0.101 m^3/s. Table 2 (column 2) lists a number of key properties, with some definitions shown in Figs. 2, 6 and 7. All results were analysed based upon the ensemble-averaged data and tested in a dimensionless manner consistent with a Froude similitude (Eq. (5)). Note that all present experiments were conducted on a smooth bed ($k_s/d_1 \approx 0$) with the same instrumentation, although it is acknowledged that the relative channel width B/d_1 differed (Table 1).

Visually some key differences were observed with breaking bores. Drastically lesser air bubble entrainment was observed at the lowest Reynolds number as illustrated in Fig. 4. Free-surface data indicated little scale effect in terms of the dimensionless maximum and conjugate water depths, and the undular bore characteristics, between two Reynolds numbers within the experimental flow conditions. Scale effects were observed for the breaking bore properties, namely in terms of free-surface rise immediately upstream of the breaking roller toe, roller length, maximum free-surface fluctuation and its delay after the bore passage. For example, an increase in Reynolds number from 9.6×10^4 to 3.5×10^5 caused a 30% decrease in maximum free-surface fluctuations and 60% decrease in time delay Δt.

Dimensionless turbulent velocity and Reynolds stress characteristics were analysed for different Reynolds numbers and the results were systematically compared. Tested characteristics included the maximum velocity fluctuation $(V_{75} - V_{25})_{max}$ and its delay Δt_v, defined as the delay in time relative to the arrival of the bore, the maximum longitudinal deceleration $(\partial V_x/\partial t)_{max}$ during the bore passage, the recirculation velocity V_{recirc} at the end of the deceleration period for breaking bores only, the maximum ensemble-median Reynolds stresses $(v_i v_j)_{max}$ and its lag ΔT_{ij}, defined as the delay in time relative to the arrival of the bore. The maximum longitudinal deceleration was calculated based upon the ensemble-averaged longitudinal velocity data during the deceleration phase. The deceleration data are presented with negative values to indicate the physical process. A key feature of breaking bores was the existence of some transient recirculation close to the channel bed immediately before the roller [19,22]. Fig. 6(A) showed an example of such a recirculation transient. Typical results are presented in Figs. 8–10. Significant differences in

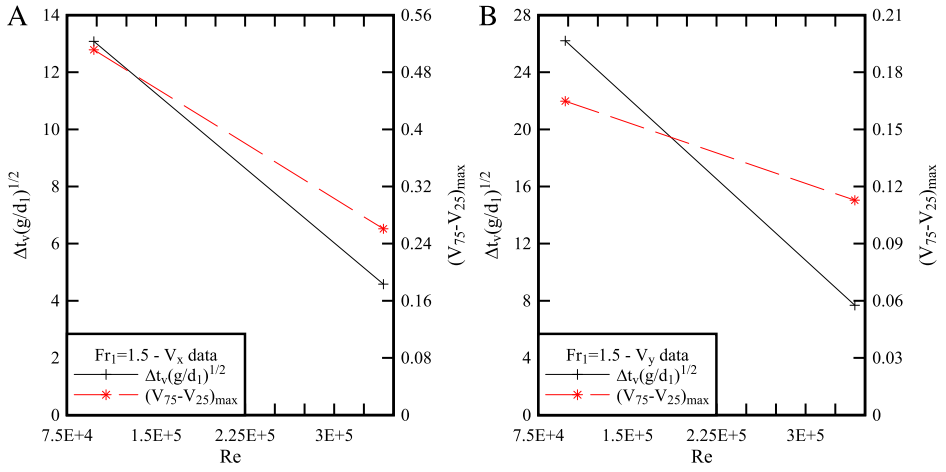

Fig. 8. Effect of Reynolds number on the maximum velocity fluctuation $(V_{75} - V_{25})_{max}$ and its delay Δt_v for breaking bores—Flow conditions $Fr_1 = 1.5, z/d_1 = 0.1$. (A, Left) Longitudinal velocity fluctuation data (B, Right) Transverse velocity fluctuation data.

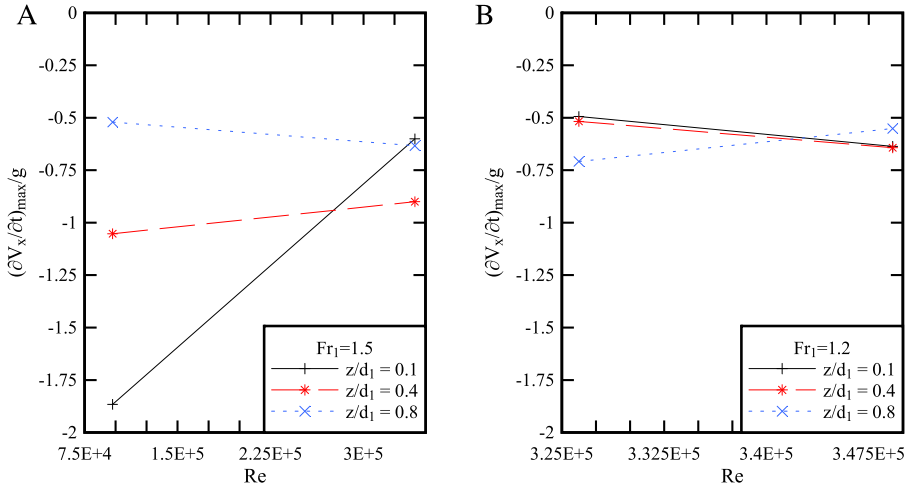

Fig. 9. Effect of Reynolds number on the maximum longitudinal deceleration at different vertical elevations. (A, Left) Breaking bore data ($Fr_1 = 1.5$) (B, Right) Undular bore data ($Fr_1 = 1.2$).

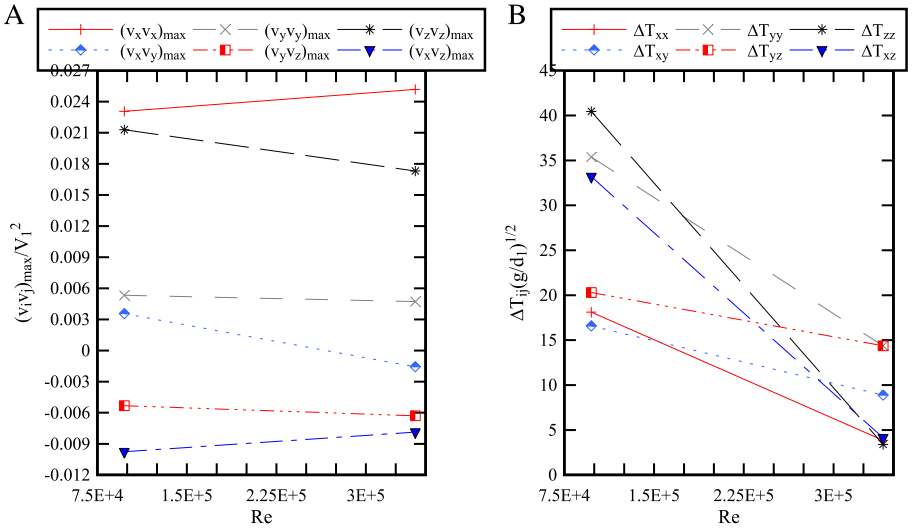

Fig. 10. Effect of Reynolds number on the maximum ensemble-median Reynolds stresses $(v_i v_j)_{max}$ and its time delay ΔT_{ij} for breaking bores—Flow conditions: $Fr_1 = 1.5, z/d_1 = 0.4$. (A, Left) Maximum ensemble-median Reynolds stresses data $(v_i v_j)_{max}$. (B, Right) Time lag data ΔT_{ij}.

maximum dimensionless velocity fluctuations and associated dimensionless time delay were observed for all three velocity components between experiments performed with the same Froude number and different Reynolds numbers. Scale effects in terms of the maximum longitudinal deceleration were most significant close to the bed ($z/d_1 = 0.1$). Next to the free-surface ($z/d_1 = 0.8$),

lesser difference was seen when the Reynolds number changed, especially in the case of breaking bores. For the turbulent Reynolds stresses, large scale effects were observed in terms of the time delay in peak Reynolds stress (Fig. 10(B)). Lesser impact was observed on the dimensionless shear stress magnitude. The change in Reynolds numbers from 9.6×10^4 to 3.5×10^5 resulted in about 30% decrease in the recirculation velocity for breaking bores of Froude number 1.5.

A summary of present scale effect analysis is presented in Table 2, with the list of tested parameters, while the experimental conditions are summarised in Table 1. Altogether the present data indicated that the extrapolation of laboratory tidal bore results is not straight forward and the up-scaling to prototype conditions might be affected by adverse scale effects.

5.3. Discussion

The present findings suggested that a number of basic free-surface properties were not affected by major scale effects based upon a Froude scaling (Table 2). The result was consistent with earlier studies [13,22]. On the other hand, the velocity characteristics and Reynolds stress results could not be up-scaled without major scale effects. While a number of studies compared laboratory and CFD data [32,33], it is believed that the present investigation is the first detailed scrutiny of the extrapolation of laboratory data to prototype conditions. Despite its relatively limited scope, the results demonstrated unequivocally the limitations of dynamic similarity and physical modelling of unsteady tidal bore flow motion (Table 2). They showed further that the selection of the criteria to test data validation and to assess scale affects is critical: e.g., the free-surface properties, the longitudinal deceleration, the velocity fluctuations, the median Reynolds stresses, the Reynolds stress fluctuations, the PDF of Reynolds stresses. Simply any mention of scale effects must be associated with the list of tested parameters [34–36] and this study presents a detailed list of outcomes (Table 2).

The experimental results stressed that some parameters, such as Reynolds stresses, are likely to be affected by scale effects, even in large-size models and small estuaries. No scale effect is observed at full scale only, using the same fluids in prototype and model: i.e., in prototype flow conditions like those illustrated in Fig. 1. Yet even some field data sets could be challenged. For example, during the studies in the Dee, Sélune and Sée Rivers [37–39], the bore flow conditions corresponded to Reynolds numbers about 4×10^5 to 2×10^6: that is, one order of magnitude lower than in large river systems like the Qiantang River (Fig. 1(B)). The previous discussion on dynamic similarity does suggest that the extrapolation of small tidal bore field results could be subjected to some form of scale effects at larger Reynolds numbers.

6. Conclusion

A tidal bore is a surge of water propagating upstream in an estuary when the macro-tidal flow turns to rising and rushes into a funnel shaped river mouth with shallow waters. It is essentially a compression wave formed in an estuarine system during the early flood tide. A series of physical experiments were conducted in a large facility to investigate the free-surface properties, unsteady velocity characteristics and Reynolds shear stresses. Both instantaneous and ensemble-averaged measurements were performed. The passage of the bore front was linked to large free-surface fluctuations, and the data showed maximum free-surface fluctuations occurring slightly after the arrival of the bore front. All velocity measurements showed a strong deceleration during the passage of the bore front, as well as large velocity fluctuations for the three velocity components at all elevations. The Reynolds stress data showed large turbulent stresses and shear stress fluctuations during the passage of bores. Maxima in normal and tangential stresses were observed shortly after the passage of a breaking bore roller toe. Overall the study demonstrated the intense turbulence and turbulent mixing under breaking and undular tidal bores.

A careful analysis of a range of dimensionless unsteady turbulent properties was conducted with two different Reynolds number ranges based upon both Froude and Morton similitudes. For both undular and breaking bores, the results demonstrated that several parameters were affected by scale effects, even in large-size models. These included the velocity and Reynolds stress fluctuations during bore propagation. The findings imply that some laboratory study data might not be up-scaled to prototype conditions without adverse scale effects. The results point to the need for further detailed field measurements, while CFD numerical models should be tested against prototype data. Future studies may further encompass tidal bores interacting with obstacles, including piers, wharfs, people, etc.…

Acknowledgements

The authors thank Professor Pierre Lubin (University of Bordeaux, France) for his personal involvement, contribution and comments. The authors acknowledge the technical assistance of Jason Van Der Gevel and Stewart Matthews (The University of Queensland). The financial support through the Australian Research Council (Grant DP120100481) is acknowledged.

References

[1] J.A. Liggett, Fluid Mechanics, McGraw-Hill, New York, USA, 1994.
[2] F.M. Henderson, Open Channel Flow, MacMillan Company, New York, USA, 1966.
[3] T.W. Sturm, Open Channel Hydraulics, in: Water Resources and Environmental Engineering Series, McGraw Hill, Boston, USA, 2001, p. 493.
[4] H. Chanson, The Hydraulics of Open Channel Flow: An Introduction, second ed., Butterworth-Heinemann, Oxford, UK, 2004, p. 630.
[5] J. Lighthill, Waves in Fluids, Cambridge University Press, Cambridge, UK, 1978, p. 504.
[6] R.A.R. Tricker, Bores, Breakers, Waves and Wakes, American Elsevier Publ. Co., New York, USA, 1965.
[7] H. Chanson, Tidal Bores, Aegir, Eagre, Mascaret, Pororoca: Theory and Observations, World Scientific, Singapore, ISBN: 9789814335416, 2011, p. 220.
[8] H. Chanson, Momentum considerations in hydraulic jumps and bores, J. Irrig. Drain. Eng. ASCE 138 (4) (2012) 382–385. http://dx.doi.org/10.1061/(ASCE)IR.1943-4774.0000409.
[9] X. Leng, H. Chanson, Breaking bore: Physical observations of roller characteristics, Mech. Res. Comm. 65 (2015) 24–29. http://dx.doi.org/10.1016/j.mechrescom.2015.02.008.
[10] J.B. Bélanger, Notes sur l'Hydraulique. ('Notes on Hydraulic Engineering.') Ecole Royale des Ponts et Chaussées, Paris, France, session 1841–1842, 1841, p. 223 (in French).
[11] R. Lemoine, Sur les ondes positives de translation dans les canaux et sur le ressaut ondulé de faible amplitude ('On the Positive Surges in Channels and on the Undular Jumps of Low Wave Height') Jl La Houille Blanche, Mar.–Apr., 1948, pp. 183–185 (in French).
[12] D.H. Peregrine, Calculations of the development of an undular bore, J. Fluid Mech. 25 (1966) 321–330.
[13] H. Chanson, Undular tidal bores: Basic theory and free-surface characteristics, J. Hydraul. Eng. ASCE 136 (11) (2010) 940–944. http://dx.doi.org/10.1061/(ASCE)HY.1943-7900.0000264.
[14] H.G. Hornung, C. Willert, S. Turner, The flow field downstream of a hydraulic jump, J. Fluid Mech. 287 (1995) 299–316.
[15] H. Chanson, N.J. Docherty, Turbulent velocity measurements in open channel bores, Eur. J. Mech. B Fluids 32 (2012) 52–58. http://dx.doi.org/10.1016/j.euromechflu.2011.10.001.
[16] X. Leng, H. Chanson, Unsteady Turbulence during the Upstream Propagation of Undular and Breaking Tidal Bores: an Experimental Investigation. Hydraulic Model Report No. CH98/15, School of Civil Engineering, The University of Queensland, Brisbane, Australia, ISBN: 978 1 74272 135 4, 2015, p. 235. pages & 4 video movies.
[17] D.G. Goring, V.I. Nikora, Despiking acoustic doppler velocimeter data, J. Hydraul. Eng. ASCE 128 (1) (2002) 117–126. Discussion: Vol. 129, No. 6, pp. 484–489.
[18] T.L. Wahl, Despiking acoustic doppler velocimeter data. Discussion, J. Hydraul. Eng. ASCE 129 (6) (2003) 484–487.

[19] C. Koch, H. Chanson, Turbulence measurements in positive surges and bores, J. Hydraul. Res. IAHR 47 (1) (2009) 29–40. http://dx.doi.org/10.3826/jhr.2009.2954.
[20] H. Chanson, Unsteady turbulence in tidal bores: Effects of bed roughness, J. Waterw. Port Coastal Ocean Eng. ASCE 136 (5) (2010) 247–256. http://dx.doi.org/10.1061/(ASCE)WW.1943-5460.0000048.
[21] B. Simon, H. Chanson, Turbulence Measurements in Tidal Bore-like Positive Surges over a Rough Bed. Hydraulic Model Report No. CH90/12, School of Civil Engineering, The University of Queensland, Brisbane, Australia, 2013, p. 176.
[22] H. Chanson, Y.H. Toi, Physical modelling of breaking tidal bores: Comparison with prototype data, J. Hydraul. Res. IAHR 53 (2) (2015) 264–273. http://dx.doi.org/10.1080/00221686.2014.989458.
[23] M.R. Spiegel, Theory and Problems of Statistics, McGraw-Hill Inc., New York, USA, 1972.
[24] N. Khezri, H. Chanson, Undular and breaking tidal bores on fixed and movable gravel beds, J. Hydraul. Res. IAHR 50 (4) (2012) 353–363.
[25] M. Brocchini, D.H. Peregrine, The dynamics of strong turbulence at free surfaces. Part 2. Free-surface boundary conditions, J. Fluid Mech. 449 (2001) 255–290.
[26] H. Chanson, Atmospheric noise of a breaking tidal bore, J. Acoust. Soc. Am. 139 (1) (2016) 12–20. http://dx.doi.org/10.1121/1.4939113.
[27] E. Wolanski, D. Williams, S. Spagnol, H. Chanson, Undular tidal bore dynamics in the daly estuary, northern Australia, Estuar. Coast. Shelf Sci. 60 (4) (2004) 629–636. http://dx.doi.org/10.1016/j.ecss.2004.03.001.
[28] H. Chanson, D. Reungoat, B. Simon, P. Lubin, High-frequency turbulence and suspended sediment concentration measurements in the garonne river tidal bore, Estuar. Coast. Shelf Sci. 95 (2–3) (2011) 298–306. http://dx.doi.org/10.1016/j.ecss.2011.09.012.
[29] C.E. Keevil, H. Chanson, D. Reungoat, Fluid flow and sediment entrainment in the Garonne river bore and tidal bore collision, Earth Surf. Process. Landf. 40 (12) (2015) 1574–1586. http://dx.doi.org/10.1002/esp.3735.
[30] A. Shields, Anwendung der Aehnlichkeitsmechanik und der Turbulenz Forschung auf die Geschiebebewegung. ('Application of similarity principles and turbulence research to bed-load movement.') Mitt. der Preussische Versuchanstalt für Wasserbau und Schiffbau, Berlin, Germany, No. 26, 1936, p. 25.
[31] M.S. Yalin, E. Karahan, Inception of sediment transport, J. Hydraul. Eng. ASCE 105 (HY11) (1979) 1433–1443.
[32] N. Khezri, Modelling Turbulent Mixing and Sediment Process Beneath Tidal Bores: Physical and Numerical Investigations (Ph.D. thesis), School of Civil Engineering, The University of Queensland, Brisbane, Australia, 2014, p. 267.
[33] B. Simon, Effects of Tidal Bores on Turbulent Mixing: a Numerical and Physical Study in Positive Surges (Ph.D. thesis), School of Civil Engineering, The University of Queensland, Brisbane, Australia, 2014, p. 259. pages & 7 movies.
[34] J. Foss, R. Panton, A. Yarin, Nondimensional representation of the boundary-value problem, in: C. Tropea, A. Yarin, J. Foss (Eds.), Handbook of Experimental Fluid Mechanics, Springer, 2007, pp. 33–83. Part A, (Chapter 2).
[35] H. Chanson, Turbulent air-water flows in hydraulic structures: Dynamic similarity and scale effects, Environ. Fluid Mech. 9 (2) (2009) 125–142. http://dx.doi.org/10.1007/s10652-008-9078-3.
[36] M.P. Schultz, K.A. Flack, Reynolds-number scaling of turbulent channel flow, Phys. Fluids 25 (2013) 13. http://dx.doi.org/10.1063/1.4791606, Paper 025104.
[37] J.H. Simpson, N.R. Fisher, P. Wiles, Reynolds stress and TKE production in an estuary with a tidal bore, Estuar. Coast. Shelf Sci. 60 (4) (2004) 619–627.
[38] D. Mouaze, H. Chanson, B. Simon, Field Measurements in the Tidal Bore of the Sélune River in the Bay of Mont Saint Michel (September 2010). Hydraulic Model Report No. CH81/10, School of Civil Engineering, The University of Queensland, Brisbane, Australia, ISBN: 9781742720210, 2010, p. 72.
[39] L. Furgerot, D. Mouaze, B. Tessier, L. Perez, S. Haquin, Suspended sediment concentration in relation to the passage of a tidal bore (Sée River Estuary, Mont Saint Michel, NW France), in: Proc. Coastal Dynamics 2013, Arcachon, France, 24–28 June, 2013, pp. 671–682.